Hyperfine-structure measurements in ^{141}Pr II and ^{143,145}Nd II by collinear laser-ion-beam spectroscopy

Li Maosheng,[1,2] Ma Hongliang,[1] Chen Miaohua,[1] Lu Fuquan,[1] Tang Jiayong,[1] and Yang Fujia[1]
[1]*Applied Ion Beam Physics Laboratory, Institute of Modern Physics, Fudan University, Shanghai 200433, People's Republic of China*
[2]*Institute of Applied Physics and Computational Mathematics, P.O. Box 8009, Beijing 100088, People's Republic of China*
(Received 7 December 1999; revised manuscript received 30 May 2000; published 11 October 2000)

Atomic spectra of singly ionized praseodymium and neodymium have been measured by means of the collinear laser-ion-beam spectroscopy. Hyperfine structures of 19 atomic transitions in the wavelength range from 560 to 590 nm were resolved and hyperfine structure constants *A* and *B* were determined for 28 levels.

PACS number(s): 32.90.+a

I. INTRODUCTION

Hyperfine structure (hfs) in atomic ions is caused by the electromagnetic interaction between the nucleus and orbital electrons. The hfs study of ions can provide certain information on nuclear structure and electronic properties of atoms. Several techniques have been developed to study hfs by using laser and ion beams. Laser excitation with a fast ion beam is a powerful method of high-precision spectroscopy. Three specific properties of a fast ion beam are useful. First, the high velocity of the ions can be utilized in measurements of atomic lifetimes [1]. Since the excitation process is selective, cascade problems are avoided and very accurate results can be obtained. Second, because of the kinematic compression, which occurs when ions are accelerated, very high spectral (sub-Doppler) resolution can be obtained with a collinear geometry. Lastly, the use of an isotope separator permits selective studies of the different isotopes. These three properties make the method of fast ion-beam-laser spectroscopy very powerful and accurate. This technique has been used to study hfs in some rare-earth ions. Some of these studies have been concerned with extracting nuclear structure information: e.g., Nd II [2,3], Sm II [4], Eu II [5]. Many reports on La II [6], Sm II [7], Eu II [8,9], and Er II [10] have dwelt on understanding the atomic structure aspects of hfs in a detailed manner.

The hyperfine energy splitting ΔE is expressed by first-order perturbation theory as the sum of the magnetic dipole term ΔE_{MD} and the electric quadrupole term ΔE_{EQ} as follows:

$$\Delta E = \Delta E_{\mathrm{MD}} + \Delta E_{\mathrm{EQ}} \tag{1}$$

$$\Delta E = \frac{1}{2}KA + \frac{\frac{3}{4}K(K+1) - I(I+1)J(J+1)}{2I(2I-1)J(2J-1)}B, \tag{2}$$

where

$$K = F(F+1) - I(I+1) - J(J+1). \tag{3}$$

The energy shift ΔE_{MD} is caused by the interaction between the internal magnetic field produced at the nucleus by orbital electrons and the nuclear magnetic dipole moment. Similarly, ΔE_{EQ} corresponds to the interaction between the electric-field gradient produced at the nucleus by the electrons and the nuclear electric quadrupole moment. *A* and *B* are the magnetic dipole and the electric quadrupole coupling constants respectively, *I*, *J*, and *F* are the nuclear spin, the electron and total angular momentum quantum numbers, respectively.

The neutron number of ^{141}Pr is a magic number 82 and the charge distribution of the nucleus is known to be nearly spherical. The nuclear quadrupole moment *Q* is very small: $Q = -0.024$ b [11]. Therefore, hyperfine interaction in Pr II is expected to be dominated by the magnetic dipole interaction, that is, $|A|$ is generally larger than $|B|$. The ^{141}Pr II lines show an hfs due to nuclear spin $\frac{5}{2}$ of the unique stable isotope ^{141}Pr. In 1989, Ginibre summarized the results of hfs measurements of Pr II [12]. The results were investigated by using the methods of Fourier transform spectroscopy and grating photographic spectroscopy. Because of Doppler broadening, Ginibre could not determine the hfs constants *A* precisely while the electric quadrupole constants *B* was neglected. In 1990, Iimura *et al.* accurately measured the hfs of two transitions $4f^3(^4I^0)5d^5G_2^0 - 4f^3(^4I^0)6p^5H_3$(601.94 nm) and $4f^3(^4I^0)5d^5G_3^0 - 4f^3(^4I^0)6p^5H_3$ (604.83 nm) of Pr II by using fast ion-beam-laser spectroscopy [13,14]. In this work, the hfs of 12 atomic transitions in the wavelength range from 560 to 590 nm were resolved and hfs constants *A* and *B* were determined for 18 levels.

Neodymium has two odd-mass stable isotopes: ^{143}Nd and

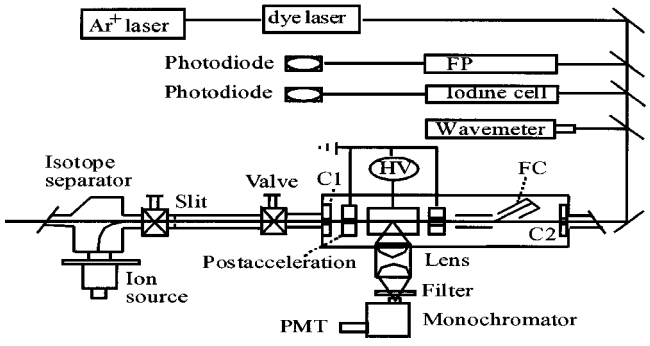

FIG. 1. The experimental setup HV, PMT, FC, FP and C1, C2 represent high-voltage power-supply, photomultiplier tube, Faraday cup, Fabry-Perot interferometer, and collimators, respectively.

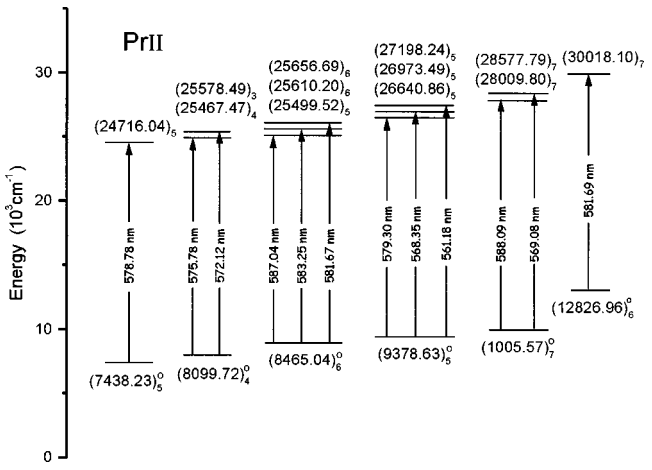

FIG. 2. Partial energy-level diagram of Pr II.

^{145}Nd. Both of them have the nuclear spin $\frac{7}{2}$. Some measurements about the hfs of Nd I were reported [15,16], but few were of Nd II. In this paper, we report our hfs measurements of Nd ions for 10 levels.

II. EXPERIMENTAL ARRANGEMENT

The experimental setup used in this work is shown in Fig. 1. The ions, produced in a low-voltage electron-impact hollow cathode ion source, were extracted by applying 30 kV and injected into an analyzing magnet (Danfysik 1080-30). Thus, an isotopically pure ion beam was selected. The ion beam passed through a vacuum flight tube and entered a chamber. Then, the beam was deflected by an electrostatic

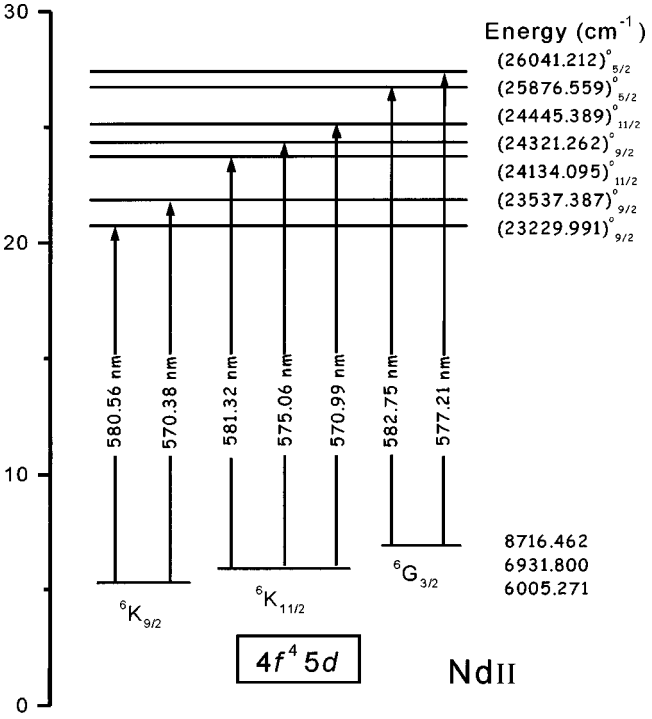

FIG. 3. Partial energy-level diagram of Nd II.

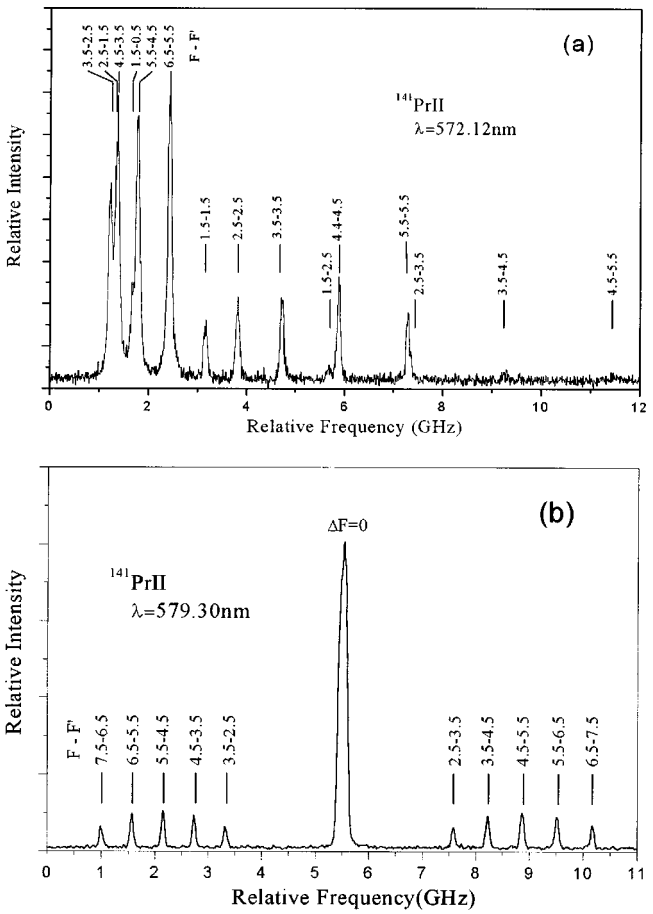

FIG. 4. Measured hyperfine spectra in Pr II. F quantum numbers are indicated in order of the lower state (F)–upper state (F').

field and detected by a Faraday cup at the far end of the chamber. The beam current was typically in the order of 0.5–1.0 μA when praseodymium chloride or neodymium chloride was used as the ion source sample.

A single-mode Coherent 899-29 ring dye laser was employed to provide light. The dye used in this work was Rhodamine 6G. The dye laser was pumped by an Ar-ion laser at a wavelength of 514.5 nm. The laser beam was steered through a Brewster window into the chamber and then through a set of apertures used to define the ion beam path. In this way, it was possible to obtain a good antipropagating overlap between the laser and ion beams in the detection region. To prevent the depletion of the metastable states by laser light before the ions entered the target chamber, a three-parts post-acceleration electrode was placed in the target chamber. Therefore it is possible to modulate the ion velocity locally. In order to avoid collisional quenching, collision-induced ion beam excitation and radiation trapping, the chamber pressure was kept below 3×10^{-5} Pa. To minimize the scattered laser light, the inner and outer surfaces of the electrode assembly and the inner surface of the target chamber were blackened, and the fluorescence photon observation and detection systems were light shielded. As a result, the scattered laser light counting rate was reduced by an order of magnitude, and was comparable to the photomultiplier tube (PMT) dark current counting rate.

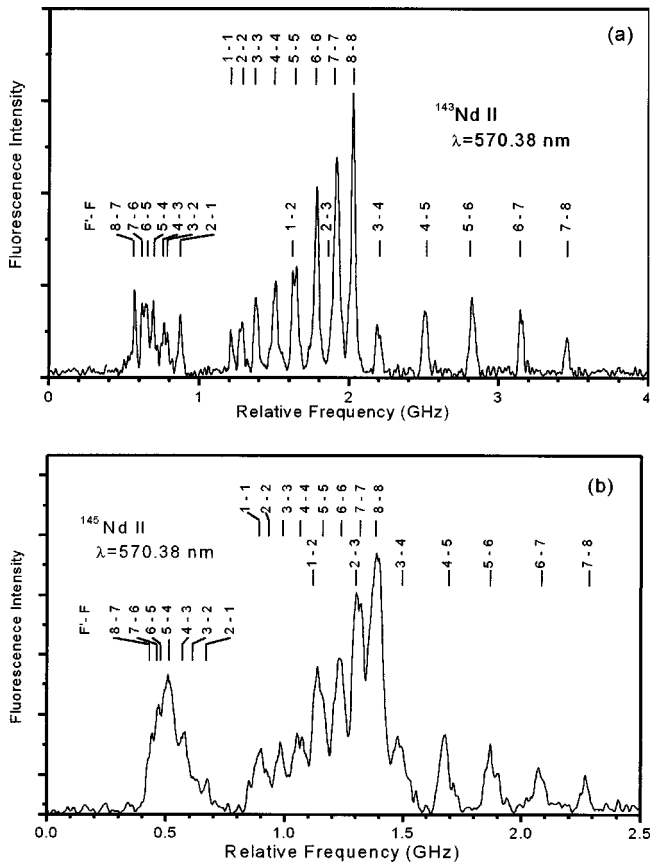

FIG. 5. Measured hyperfine spectra in Nd II. F quantum numbers are indicated in order of the upper state (F')–lower state(F).

The linearity of the laser frequency versus the relative direct-current level from the laser control box is, however, not sufficient to be used directly for evaluation of the recorded spectra. To obtain the frequency scale, part of the laser was directed into a Fabry-Perot interferometer. The free spectral range (FSR) of the interferometer was calibrated using an iodine spectrum measured over a 30 GHz range. This procedure yielded an FSR of 146.5 ± 0.1 MHz. Another part of the laser light was directed into an iodine cell for a simultaneous recording of an iodine spectrum for the absolute frequency scale.

The fluorescence photons were collected perpendicularly to the beam axis through an 11 cm focal-length lens. They were then analyzed using a grating monochromator and detected by a PMT. Data acquisition was performed using two multichannel analyzers (MCAs). Signals allowed the ramp voltage from the dye laser control unit to be digitized and recorded in the MCAs.

III. EXPERIMENTAL RESULTS AND ANALYSIS

The energy levels diagram of Pr II and Nd II relevant to this investigation are shown below in Figs. 2 and 3, respectively. The excitation energies are from Ref. [17].

A typical hyperfine spectrum for Pr II 572.12 nm and 579.30 nm lines are shown below in Fig. 4 and for ^{143}N II, ^{145}Nd II 570.38 nm lines are shown below in Fig. 5. The measured hyperfine spectra give information on the magnetic dipole coupling constant A and the electric quadruple coupling constant B of the upper and the lower levels. These overdetermined equation systems were solved according to the least-squares criteria.

For each scan, the iodine absorption spectrum, Fabry-Perot (FP) fringes, and the hyperfine spectrum obtained from the laser-induced fluorescence signals were recorded simultaneously. The first two data sets were used to check that the run had been performed correctly. The FP fringes were used to establish the frequency scale. The positions of the fringes were determined by fitting Gaussian functions of equal height and equal width to the recorded peaks. To utilize the fact that the fringes are equidistant in the frequency domain, the peak positions as a function of the fringe number were fitted to a polynomial, usually of degree three. This frequency calibration function was used to determine the frequencies corresponding to the peak positions found for the hyperfine peaks. These spectral lines were also fitted by Gaussian line shape. The fitting procedure gave statistical errors composed of both the uncertainty in the peak position determination and the uncertainty originating from the frequency calibration function.

The analysis of the recorded curves with respect to hfs is subject to possible systematic errors caused by experimental deficiencies, such as laser frequency calibration, uncertainties in determining the centers of the peaks in the hfs spectrum and the ion velocity distribution. The line broadening is partly due to the moderate quality of the ion beam. The 30 kV acceleration voltage had a ripple of 5 V. Some additional energy dispersion may arise from plasma ion source instabilities. This energy fluctuation leads to a spread of the velocity distribution. The statistical error on the relative frequency was typically 1 MHz. The final errors of A and B were typically 1 and 5 MHz, respectively. Results of Pr II are shown in Table I with the corresponding reference values. Measured hfs constants A and B in ^{143,145}Nd II are shown in Table II.

In the comparison between the present and reference values for 18 levels in Pr II the magnetic dipole coupling constants A are in good agreement with the Ginibre's result for 17 levels. For the $^5H_3$ level, the value of A differs from the Ginibre's result beyond experiment error. Concerning the electric quadruple coupling constants B, there are no reference values for comparison. For Nd II it is evident that the magnetic dipole coupling constants A were well determined, and the electric quadruple coupling constants B, however, were rough. We also calculated the values of A^{145}/A^{143} for each level to compare with the values of $(\mu_1^{145} I^{143})/(\mu_1^{143} I^{145})[=0.616(5)$, according to the value in Ref. [18]]. It suggested that the hyperfine anomaly is relatively small ($^{143}\Delta^{145} \approx -1\%$).

IV. CONCLUSION

The hyperfine structures of 18 levels in Pr II and 10 levels in Nd II have been measured by means of the collinear laser-ion-beam spectroscopy. For Pr II, the magnetic dipole coupling constants A are in good agreement with the Ginibre's

TABLE I. Measured hyperfine constants A and B in Pr II, A_G are from Ginibre [12].

λ (nm)	Energy (cm^{-1})	A (MHz)	B (MHz)	A_G (MHz)
578.78	7438.23	709.3±1.2	19.5±6.0	714±6
	24 716.04	735.0±1.1	15.9±3.5	732±22
581.67	8465.04	572.9±1.2	−4.1±7.0	
	25 656.69	656.4±1.0	−10.0±2.1	657±46
587.04	8465.04	574.1±1.3	−8.0±6.0	
	25 499.52	632.1±1.3	−14.5±4.1	639±55
583.25	8465.04	574.8±1.0	−3.1±5.0	
	25 610.20	543.2±0.7	−7.2±3.1	546±46
572.12	8099.72	768.4±1.2	37.9±6.8	
	25 578.49	1031.6±2.2	12.2±6.6	891±17
575.78	8099.72	773.1±1.3	31.5±6.3	
	25 467.47	736.2±1.5	16.2±6.6	732±67
561.18	9378.63	612.7±1.5	9.3±9.7	
	27 198.24	583.3±1.1	−4.6±4.3	600±55
568.35	9378.63	613.7±1.5	8.1±9.0	
	26 973.49	601.7±1.2	−1.6±3.7	612±22
579.30	9378.63	615.1±1.3	10.0±9.1	
	26 640.86	619.1±1.0	5.4±4.0	588±54
588.09	11 005.57	546.3±1.3	10.3±9.9	
	28 009.80	558.2±1.0	5.4±4.0	576±40
569.08	11 005.57	547.0±1.5	9.1±9.8	
	28 577.79	530.8±1.1	−4.9±5.4	537±16
581.69	12 826.94	487.3±1.0	−17.4±5.6	489±46
	30 018.10	525.9±1.1	4.0±3.7	495±40
mean	8465.04	573.9±0.7	−5.1±3.5	576±5
	8099.72	770.8±0.8	34.7±4.6	768±13
	9378.63	613.8±0.8	9.1±5.4	612±11
	11 005.57	546.7±1.0	9.7±7.0	558±40

TABLE II. Measured hyperfine constants A and B in ^{143,145}Nd II.

Level (cm^{-1})	J	λ (nm)	A (MHz) ^{143}Nd II	A (MHz) ^{145}Nd II	B (MHz) ^{143}Nd II	B (MHz) ^{145}Nd II
8716.462	3/2	582.75	−393.6±0.8	−247.0±1.6	9.2±7.0	−0.8±4.3
		577.21	−394.9±0.6	−244.7±0.8	1.1±6.5	−0.5±3.6
		mean	−394.3±0.5	−245.8±0.9	5.1±4.8	−0.6±2.8
25 876.559	5/2	582.75	−45.5±1.0	−28.3±0.4	−22.1±7.6	−9.7±3.2
26 041.212	5/2	577.21	−70.3±0.4	−43.4±0.5	−6.3±5.4	−2.3±4.2
6005.271	9/2	580.65	−200.2±1.5	−124.1±1.4	−120.5±8.1	65.7±11.8
		570.38	−199.8±1.4	−124.0±1.5	−111.9±5.7	68.0±17.3
		mean	−200.2±1.0	−124.1±1.0	−116.2±5.0	66.7±10.5
23 229.991	9/2	580.65	−197.2±0.7	−121.1±1.2	−106.1±9.4	−52.0±9.1
23 537.387	9/2	570.38	−175.5±1.1	−109.8±1.4	−57.9±10.4	−31.4±5.7
24 134.095	11/2	581.32	−148.0±1.6	−91.95± 2.7	46.6±9.2	23.1±8.3
24 321.262	9/2	575.06	−163.2±0.8	−100.9±0.6	−180.6±4.2	−103.1±3.1
24 445.389	11/2	570.99	−134.7±0.7	−84.2±1.3	−211.3±4.6	97.0±0.7
6931.800	11/2	581.32	−151.8±0.9	−94.9±2.7	58.8±8.0	29.4±3.1
		575.06	−150.9±0.6	−93.1±0.7	54.9±3.6	28.6±2.5
		570.99	−149.7±0.7	−92.5±1.6	49.8±7.0	26.3±2.3
		mean	−150.8±0.4	−93.5±1.1	54.5±2.6	28.1±1.5

result for 17 levels, but the accuracy has been improved by one order of magnitude. Concerning the electric quadruple coupling constants *B*, there are no reference values for comparison. Neither theoretical nor experimental values are available for comparison. The hyperfine constants *B* is much smaller than the hyperfine constants *A*. These results are consistent with the fact that the nuclear quadrupole moment *Q* of ^{141}Pr II is very small. For ^{143,145}Nd II there are no reference values for comparison.

ACKNOWLEDGMENTS

This work was supported by the National Science Foundation of China under Grant No. 19874015 and also by Zhonglu-Bohr.

[1] Shi Wei, Lu Fuquan, Wu Songmao, Shi Peixiong, Yang Jianjun, Song Linggen, Tang Jiayong, and Yang Fujia, Phys. Rev. A **43**, 1451 (1991).
[2] Lu Fuquan, Wu Songmao, Wang Yansen, Shi Wei, Shi Peixiong, Song Linggen, Yang Jianjun, Tang Jiayong, and Yang Fujia, Phys. Rev. A **44**, 1843 (1991).
[3] Ma Hongliang, Shi Wei, Yan Bin, Li Yong, Fang Dufei, Lu Fuquan, Tang Jiayong, and Yang Fujia, J. Phys. B **30**, 3355 (1997).
[4] K. Dörschel, H. Hühnermann, E. Knobl, Th. Meier, and H. Wagner, Z. Phys. A **302**, 359 (1981).
[5] K. Dörschel, W. Heddrich, H. Hühnermann, E. W. Peau, and H. Wagner, Z. Phys. A **317**, 233 (1984).
[6] C. Hohle, H. Hünnermann, and H. Wagner, Z. Phys. A **304**, 279 (1982).
[7] L. Young, W. J. Childs, H. G. Berry, and T. Dinneen, Phys. Rev. A **36**, 2148 (1987).
[8] A. Arnesen, A. Bengston, R. Hallin, O. Staaf, and L. Wand, Phys. Scr. **24**, 747 (1981).
[9] A. Sen and W. J. Childs, Phys. Rev. A **36**, 1983 (1987).
[10] U. Nielsen, K. T. Cheng, and H. Ludyigsen, Phys. Scr. **39**, 776 (1986).
[11] K. D. Böklen, T. Bossert, W. Foerster, H. H. Fuchs, and G. Nachtsheim, Z. Phys. A **274**, 195 (1975).
[12] A. Ginibre, Phys. Scr. **39**, 694 (1989).
[13] H. Iimura, Y. Nakahara, S. Ichikawa, K. Kotani, M. Wakasugi, and T. Horiguchi, J. Phys. Soc. Jpn. **59**, 4208 (1990).
[14] H. Iimura, Y. Nakahara, S. Ichikawa, M. Kubota, and T. Horiguchi, Phys. Rev. C **50**, 661 (1994).
[15] W. J. Childs, Phys. Rev. A **44**, 760 (1991).
[16] P. Aufmuth, A. Bernard, M. Deckwer, E.-G. Kopp and A. Steudel, Z. Phys. D: At., Mol. Clusters **23**, 19 (1992).
[17] W. C. Martin, R. Zalubas, and L. Hagan, *Atomic Energy Levels. The Rare Earth Elements*, Natl. Bur. Stand. Ref. Data Ser., Natl. Bur. Stand. (U.S.) Circ. No. 60 (U.S. GPO, Washington D.C. 1978).
[18] P. Raghavan, At. Data Nucl. Data Tables **42**, 189 (1989).